Nature and Role of Bridged Carbonyl Intermediates in the Ultrafast Photoinduced Rearrangement of $Ru_3(CO)_{12}$

Elizabeth A. Glascoe, Matthias F. Kling,† Jennifer E. Shanoski, and Charles B. Harris*

Department of Chemistry, University of California, and Chemical Sciences Division, Lawrence Berkeley National Laboratory, Berkeley, California 94720

Received September 15, 2005

The photochemistry of the trimetal cluster $Ru_3(CO)_{12}$ was investigated on the ultrafast time scale using UV−vis pump, infrared probe spectroscopy in order to study the transient intermediates formed upon photoexcitation. The dynamics of these intermediates can only be unambiguously identified by monitoring the small but distinct infrared absorptions of bridging carbonyls. The nature and role of bridging carbonyl intermediates in the photochemistry of $Ru_3(CO)_{12}$ in both coordinating and noncoordinating solvents is discussed. In an inert solvent such as cyclohexane, photoexcitation of $Ru_3(CO)_{12}$ with 400 nm light produces two different species that have never been observed simultaneously. The first species is a carbonyl loss complex with a bridging carbonyl that forms in 134 ± 22 ps and survives beyond 800 ps; the second species is a bridging carbonyl complex with one metal−metal bond cleaved that forms in 23 ± 3 ps and has a lifetime of 60 ± 5 ps. When 266 nm light was used to photoexcite the cluster, both species exhibit similar dynamics. This is the first time multiple bridging carbonyl intermediates have been observed simultaneously for this cluster, and this observation resolves an inconsistency in the literature. Interestingly, in neat solutions of THF only one feature was observed in the bridging carbonyl region, yet the dynamics of the feature and density functional theory (DFT) results indicate that there are, in fact, two bridging carbonyl complexes with overlapping bands. These results were surprising, as it was previously unknown whether THF would block formation of bridging carbonyl complexes by solvating and stabilizing the coordinatively unsaturated metal.

I. Introduction

The transition-metal cluster $Ru_3(CO)_{12}$ is widely used in photoactivated synthesis, and therefore its rearrangement and decomposition dynamics are not only of fundamental interest but also of industrial importance.[1,2] In general, photoactivation of this cluster allows for systematic control in synthetic procedures by breaking only specific types of bonds in the complex when a particular wavelength of light is used.[2,3] A particularly interesting aspect of this system is that it exhibits unique dynamics, due to its trimetal infrastructure, that are not possible in corresponding metal monomers or dimers. The structure of $Ru_3(CO)_{12}$ and of some of its photochemical intermediates, as well as the main reaction channels, have been investigated previously in matrices and solutions using laser flash photolysis in combination with visible or infrared spectroscopy.[4−13] It is evident from a thorough examination of previous studies that many fundamental aspects, including the wavelength specificity of bond cleavage and the nature of the transients formed, are unclear. The ambiguity in the current picture for $Ru_3(CO)_{12}$ reactivity prompted an investigation of this reaction using spectroscopic techniques that allow for detection of transient species with high sensitivity and ultrafast time resolution.

Previous experimental analysis and theoretical modeling indicated that $Ru_3(CO)_{12}$ has a triangular arrangement of the metal atoms with four terminal carbonyl groups attached to each metal (see Figure 1, starting complex).[5,11] The UV−vis spectrum has two prominent absorption bands: the first centered at 390 nm and the second centered at 238 nm. Electronic absorption studies indicate that the lower energy band (390 nm) of $Ru_3(CO)_{12}$ originates from $\sigma^* \leftarrow \sigma$ transitions in metal d orbitals,[14,15]

* To whom correspondence should be addressed. E-mail: cbharris@berkeley.edu.

† Present address: FOM Institute for Atomic and Molecular Physics (AMOLF), Kruislaan 407, 1098 SJ Amsterdam, The Netherlands.

(1) (a) Richmond, M. G. *Coord. Chem. Rev.* **2004**, *248*, 881. (b) Dyson, P. J.; McIndoe, S. J. *Transition Metal Carbonyl Cluster Chemistry*; Gordon and Breach: Amsterdam, The Netherlands, 2000. (c) Michelin Lausarot, P.; Vaglio, G. A.; Valle, M. *J. Organomet. Chem.* **1984**, *275*, 233. (d) Kakiuchi, F.; Matsumoto, M.; Tsuchiya, K.; Igi, K.; Hayamizu, T.; Chatani, N.; Murai, S. *J. Organomet. Chem.* **2003**, *686*, 134. (e) Meijer, R. H.; Ligthart, G. B. W. L.; Meuldijk, J.; Vekemans, J. A. J. M.; Hulshof, L. A.; Mills, A. M.; Kooijman, H.; Spek, A. L. *Tetrahedron* **2004**, *60*, 1065. (f) Leadbeater, N. E. *J. Chem. Soc., Dalton Trans.* **1995**, *18*, 2923. (g) Edwards, A. J.; Leadbeater, N. E.; Lewis, J.; Raithby, P. R. *J. Organomet. Chem.* **1995**, *503*, 15.

(2) Wuu, Y. M.; Bentsen, J. G.; Brinkley, C. G.; Wrighton, M. S. *Inorg. Chem.* **1987**, *26*, 530.

(3) Bentsen, J. G.; Wrighton, M. S. *J. Am. Chem. Soc.* **1987**, *109*, 4530.

(4) Bentsen, J. G.; Wrighton, M. S. *J. Am. Chem. Soc.* **1987**, *109*, 4518.

(5) Churchill, M. R.; Hollander, F. J.; Hustchinson, J. P. *Inorg. Chem.* **1977**, *16*, 2655.

(6) Desrosiers, M. F.; Ford, P. C. *Organometallics* **1982**, *1*, 1715.

(7) Desrosiers, M. F.; Wink, D. A.; Ford, P. C. *Inorg. Chem.* **1985**, *24*, 1.

(8) Desrosiers, M. F.; Wink, D.; Trautman, R.; Friedman, A. E.; Ford, P. C. *J. Am. Chem. Soc.* **1986**, *108*, 1917.

(9) Dibenedetto, J. A.; Ryba, D. W.; Ford, P. C. *Inorg. Chem.* **1989**, *28*, 3503.

(10) Grevels, F. W.; Klotzbucher, W. E.; Schrickel, J.; Schaffner, K. *J. Am. Chem. Soc.* **1994**, *116*, 6229.

(11) Hunstock, E.; Mealli, C.; Calhorda, M. J.; Reinhold, J. *Inorg. Chem.* **1999**, *38*, 5053.

(12) Johnson, B. F. G.; Lewis, J.; Twigg, M. V. *J. Organomet. Chem.* **1974**, *67*, C75.

(13) Vergeer, F. W.; Hartl, F.; Matousek, P.; Stufkens, D.; Towrie, M. *Chem. Commun.* **2002**, 1220.

(14) Tyler, D. R.; Levenson, R. A.; Gray, H. B. *J. Am. Chem. Soc.* **1978**, *100*, 7888.

10.1021/om050795o CCC: $33.50
Publication on Web 12/22/2005

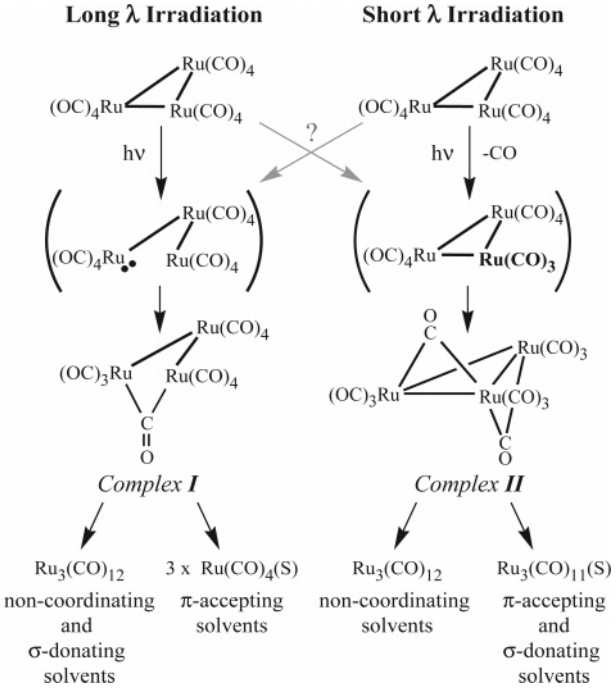

Figure 1. Summary of the solvent- and wavelength-dependent photochemistry of Ru_3CO_{12} clusters as it is currently understood. See the text for details and references.

so that excitation with visible light in this region results in heterolytic cleavage of one of the Ru−Ru bonds.[6,12,16] The complex formed retains the three-metal cluster unit and exhibits a bridging carbonyl to accommodate the redistribution of charge (see Figure 1, complex **I**). This bridging carbonyl transient and its dynamics have been characterized in a previous study using ultrafast infrared spectroscopy, by its signature bridging carbonyl stretching frequency of ca. 1850 cm^{-1}.[13] The subsequent photochemistry has been extensively studied, and it is generally observed that the solvent plays a key role in determining the final photoproducts (see Figure 1, long λ irradiation).[6−8,16] In noncoordinating solvents, i.e., solvents that are not able to stabilize the intermediate, such as alkanes, it is observed that the starting material is eventually re-formed.[6,16] In the presence of π-back-bonding ligands, for example CO and phosphines, fragmentation of the photoexcited cluster and formation of three identical monomer units each containing a π-back-bonding molecule is observed.[6−8,16] Interestingly, in the presence of molecules, such as THF, that can only donate electron density to the metal in a σ-bonding fashion, photofragmentation is blocked and the starting material is regenerated; the reasons for this behavior remain unclear.[6−8]

The short-wavelength, high-energy peak at 238 nm in the UV−vis absorption spectrum of $Ru_3(CO)_{12}$ has been characterized as a metal to ligand charge transfer (MLCT) excitation that ultimately results in loss of one carbonyl group in solution or in a matrix.[3,14] Again, the solvent molecules play a key role in determining the final photoproducts. Noncoordinating solvents such as alkanes cannot stabilize the coordinatively unsaturated cluster; therefore, the complex is internally stabilized by a bridging carbonyl between two of the metal atoms (Figure 1, complex **II**). The bridging carbonyl has been observed in a 90 K matrix and in solution in the 1830−1850 cm^{-1} region.[3,10] In coordinating solvents, both σ-donating and π-back-bonding, the solvent molecule binds and forms the photosubstituted product $Ru_3(CO)_{11}S$ (S = solvent molecule). The lifetime of this product depends on its thermodynamic stability with respect to the starting material and the availability of CO to replace the solvent S and re-form the original cluster.[3,7−9]

Despite the wealth of information provided by previous studies, some particularly important details of the photochemistry of $Ru_3(CO)_{12}$ are unresolved. First, the time scales of formation and decay for the CO loss transient have not been determined and the structures of both bridging carbonyl complexes discussed above are uncertain. Second, a clear picture of the structure and dynamics of the cluster in σ-donating solvents does not exist. Finally, a careful perusal of the literature exposes an inconsistency concerning the number and type of photoproducts formed with disparate wavelengths of excitation, as is discussed below. Photofragmentation products are formed upon excitation with both visible and ultraviolet light (in the presence of π-back-bonding ligands), and a constant quantum yield between 313 and 436 nm was observed.[7,8,16] In contrast, the quantum yields for photosubstitution products resulting from excitation in this spectral region tend to increase dramatically with decreasing wavelength.[7,8] The pathways for the generation of two different products that are formed at the same wavelength remain unexamined. It has been suggested that photofragmentation is a result of the photochemistry that starts with photodissociation of a carbonyl.[10] It was hypothesized by others that both the carbonyl loss channel and the metal−metal cleavage channel are accessed at all wavelengths in this region.[7,8]

Most studies have suggested that a bridging carbonyl complex (regardless of whether it is derived from the CO loss or metal−metal cleavage channel) is formed in noncoordinating solvents.[6−8,16] A few studies have directly observed a bridging carbonyl complex, and each study used a different wavelength of excitation.[3,10,13] It is important to point out that in every study in which a bridging carbonyl complex was observed, only one species could be detected. This is inconsistent with results that suggest multiple photoproducts, derived from multiple bridging carbonyl complexes, are formed at a single excitation wavelength.[7,8] In addition, different vibrational frequencies were reported for the bridging carbonyl in each study, possibly due to experimental limitations of wavelength resolution and detection sensitivity. Despite all the previous work to characterize the photochemistry of $Ru_3(CO)_{12}$, the structure and number of bridging carbonyl complexes formed at various excitation wavelengths remain in dispute.

We investigated the primary photoproducts of $Ru_3(CO)_{12}$ excited at 266 and 400 nm in solutions of cyclohexane and THF using a combination of ultrafast infrared absorption spectroscopy and DFT modeling. The goal of this study was to gain a more complete understanding of the transient photoproducts formed upon UV and visible excitation of $Ru_3(CO)_{12}$. In contrast with previous studies, we were able to spectroscopically resolve all relevant bridging carbonyl intermediates and have found that two types of bridging carbonyl complexes are in fact present after both 266 and 400 nm excitation. What follows is a clearer picture of the ultrafast dynamics of the cluster upon photoexcitation that resolves inconsistencies in the literature and clarifies open questions on the photochemistry of transition-metal clusters.

The paper is organized as follows: experimental and theoretical methods are described in section II, the results on the photochemistry of $Ru_3(CO)_{12}$ in cyclohexane and THF solution after 266 and 400 nm irrediation are given in section IIIA, and the DFT calculations are presented in section IIIB. In section

(15) Delley, B.; Manning, M. C.; Ellis, D. E.; Berkowitz, J.; Trogler, W. C. *Inorg. Chem.* **1982**, *21*, 2247.
(16) Malito, J.; Markiewicz, S.; Poe, A. *Inorg. Chem.* **1982**, *21*, 4335.

IV, the dynamics of the photoexcited clusters with noncoordinating and coordinating solvents is discussed. We finally conclude our results on the photochemistry of $Ru_3(CO)_{12}$ in section V.

II. Methods

A. Samples. $Ru_3(CO)_{12}$, spectroscopic grade cyclohexane, and anhydrous THF were purchased from Sigma-Aldrich and used without further purification. Dilute solutions (1−2 mM) were prepared and filtered.

B. Femtosecond Infrared Spectroscopy. The experimental apparatus has been described in detail elsewhere.[17] In brief, the setup consists of a Ti:sapphire regenerative amplifier (Spectra-Physics, Spitfire) seeded by a Ti:sapphire oscillator (SpectraPhysics, Tsunami) to produce a 1 kHz train of 100 fs pulses centered at 800 nm with an average pulse power of 0.9 mJ. The output of this system is split and used to generate 266 (0.3 μJ at sample) or 400 nm (1.6 μJ at sample) pump pulses and to pump a home-built optical parametric amplifier (OPA) able to deliver mid-IR probe pulses tunable from 3 to 6.0 μm with a spectral width of 200 cm^{-1} and a pulse duration of around 150 fs. A computer-controlled translation stage (Klinger) allows for variable time delays up to 800 ps between pump and probe pulses.

The sample is flowed using a mechanical pump through a stainless steel cell (Harrick Scientific) fitted with 1.5 mm thick MgF_2 windows and an optical path length of 350 μm. The bleaching of sample molecules due to photoinduced decomposition was estimated to be smaller than 5% within 5 h of laser operation—a typical time scale for continuous data collection. The sample cell is moved by computer-controlled translational stages (Standa) in space after each measured spectrum to ensure that absorptions are not masked or enhanced due to sample burning onto the windows. Reference and signal IR beams are sent along a parallel path through a computer-controlled spectrograph (Acton Research Corp., SpectraPro-150) and detected by a 2 × 32 element MCT-array IR detector (InfraRed Associates, Inc.) and a high-speed signal acquisition system and data acquisition software (Infrared Systems Development Corp.) with a resolution of ca. 3 cm^{-1}. Collected signals are typically averaged over 1000 laser shots to account for shot-to-shot fluctuations of the laser. Differences in optical density (ΔOD) as small as 2×10^{-5} can be observed in the experiments after ca. 10−15 s of data collection.

C. Data Analysis Methods. Time scales for reactant and product evolution were determined by fitting the peak amplitude or peak area to a sum of exponentials using the Levenberg−Marquart method. Peak areas were determined by fitting spectra to a sum of Voigt functions and calculating the areas which were used to resolve the kinetics of overlapping absorption bands. This method will be referred to as the area fitting method. Peaks that are indistinguishable due to extensive overlap could not be fit to Voigt functions. To gain some insight into the dynamics of these heavily overlapped peaks, the infrared intensity at a single wavenumber was fit, and this method will be referred to hereafter as the trace-fitting method. Note that the kinetics at a single wavenumber may be attributed to the dynamics of multiple peaks in close proximity and the time scales determined using this method may not be as accurate as those measured using the peak areas.[18]

D. Density Functional Theory Calculations. Density functional theory (DFT) calculations have been used to assist in the characterization of the intermediate species and to facilitate an understanding of the dynamical behavior observed. The results from DFT calculations described here were carried out with Gaussian03[19] using Becke's three-parameter exchange-correlation energy[20] combined with the Lee−Yang−Parr correlation functional,[21] B3LYP.[22] Generic basis sets used consisted of the LANL2DZ core potential[23] for ruthenium and 6-31G(d) (basis set A), and 6-31+G(d) (basis set B) basis sets for lighter atoms. Frequency calculations were carried out in order to ensure that configurations obtained correspond to minima on the potential energy surface. All calculated frequencies were scaled by a factor of 0.9614.[24] DFT calculations have been shown to be reliable in calculations of transition-metal complex structures, vibrational frequencies, and energetics.[25]

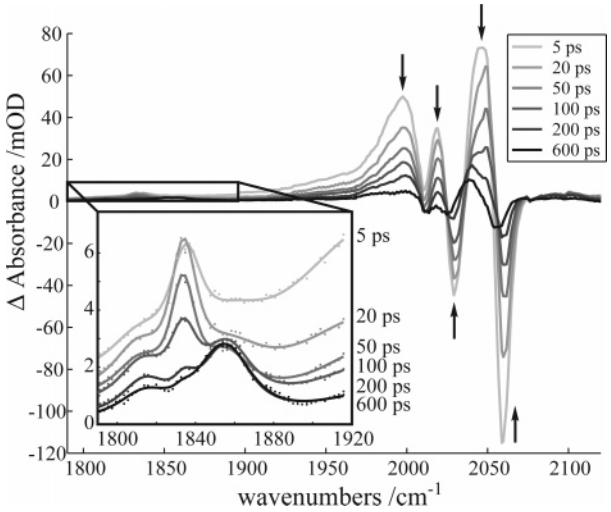

Figure 2. $Ru_3(CO)_{12}$ in cyclohexane excited with 400 nm light (1.6 μJ). Spectra in the inset are fits overlaid on the raw data. Arrows indicate changes with increasing delay time.

III. Results

A. Femtosecond UV Pump/IR Probe Spectroscopy of $Ru_3(CO)_{12}$. Data have been obtained on the photochemistry of $Ru_3(CO)_{12}$ in neat cyclohexane, a weakly coordinating solvent, and neat THF, a Lewis base. All spectra are represented as infrared difference spectra in which a spectrum of the parent molecule before photoexcitation is subtracted from a spectrum of the photoexcited complex such that negative peaks represent parent molecules that have been depleted (hereafter referred to as the parent bleach) and positive peaks represent new species that have been formed at designated times after photoexcitation.

(a) Cyclohexane Results. Figure 2 contains the IR difference spectra for $Ru_3(CO)_{12}$ in cyclohexane after photoexcitation with 400 nm light (1.6 μJ). The large peaks between 1930 and 2100 cm^{-1} represent the IR absorptions of the terminal carbonyls from all species formed. It is difficult to extract much useful information from this region, as there are a multitude of carbonyl ligands from each photoexcited species that produce a spectrum of overlapping, indistinguishable peaks in solution.[3] The kinetics of the peaks in this region were determined with the trace-fitting method, and respective time constants are reported in Table 1. In addition, three small peaks at 1815, 1833, and 1857 cm^{-1} can be discerned and are shown in the inset of Figure 2. These

(17) Shanoski, J. E.; Payne, C. K.; Kling, M. F.; Glascoe, E. A.; Harris, C. B. *Organometallics* **2005**, *24*, 1852.

(18) All errors presented reflect 95% confidence intervals. In the case of the area-fitting method, the errors presented do not take into account the goodness of fit of the Voigt function to the raw data.

(19) Frisch, M. J.; et al. *Gaussian 03, Revision C.02*; Gaussian, Inc.: Wallingford, CT, 2004.

(20) Becke, A. D. *J. Chem. Phys* **1993**, *98*, 5648.

(21) Lee, C.; Yang, W.; Parr, R. G. *Phys. Rev. B* **1988**, *37*, 785.

(22) Stephens, P. J.; Devlin, G. J.; Chabalowski, C. F.; Frisch, M. M. *J. Phys. Chem.* **1994**, *98*, 11623.

(23) Hay, P. J.; Wadt, W. R. *J. Chem. Phys.* **1985**, *82*, 299.

(24) Scott, A. P.; Radom, L. *J. Phys. Chem.* **1996**, *100*, 16502.

(25) Niu, S.; Hall, M. B. *Chem. Rev.* **2000**, *100*, 353.

Table 1. Exponential Fitting Parameters of Product and Bleach Recovery Peaks from $Ru_3(CO)_{12}$ in Cyclohexane Excited with 266 or 400 nm Light

peak/cm^{-1}	$\tau_{400\ nm}$/ps		$\tau_{266\ nm}$/ps	
Product Peaks in Cyclohexane				
1833	23 ± 3	rise	15 ± 2	rise
	60 ± 5	decay	63 ± 5	decay
1857	134 ± 22	rise	158 ± 42	rise
	ns	decay	ns	decay
1935	12 ± 1	decay	22 ± 4	decay
	128 ± 24	decay	206 ± 72	decay
1950	7.8 ± 0.3	decay	8 ± 1	decay
	101 ± 1	decay	67 ± 9	decay
1999	13 ± 1	decay	26 ± 2	decay
	137 ± 2	decay	152 ± 6	decay
2018	97 ± 1	decay	6 ± 1	rise
			94 ± 1	decay
2039	17 ± 1	decay	22 ± 1	rise
			291 ± 26	decay
2049	2 ± 2	rise	6.3 ± 0.2	decay
	88 ± 1	decay	83.2 ± 04	decay
2092	262 ± 10	decay	27 ± 16	decay
			170 ± 29	decay
2104	325 ± 9	decay	201 ± 8	decay
Bleach Peaks in Cyclohexane				
2029	108.5 ± 0.2	rise	6 ± 1	decay
			58 ± 1	rise
2060	13 ± 1	rise	37 ± 1	rise
	68 ± 3	rise	164 ± 17	rise

peaks originate from bridging CO stretching frequencies which typically appear in the region between 1800 and 1900 cm^{-1}.[3,10,13]

The dynamics of the largest bridging carbonyl peak centered at 1833 cm^{-1} were determined with the area-fitting method to have an exponential rise time of 23 ± 3 ps and a decay of 60 ± 5 ps, shown in Figure 3a. Figure 3b shows the temporal evolution of the area of the peak centered at 1857 cm^{-1}. In nearly all experimental data, partial overlap of the terminal carbonyl band, centered at ca. 1935 cm^{-1}, with the 1857 cm^{-1} band was observed. The decay of the terminal carbonyl band was taken into account in our triexponential fit of the 1857 cm^{-1} peak by using a fixed decay time of 12 ps, which represents the vibrational cooling of the neighboring terminal carbonyl band. The rise time of 134 ± 22 ps and a long slow decay of ca. 5 ns reflect the sole dynamics of the bridging carbonyl species. Due to the small signal, the kinetics of the small peak at 1815 cm^{-1} were extremely difficult to obtain, preventing further analysis.

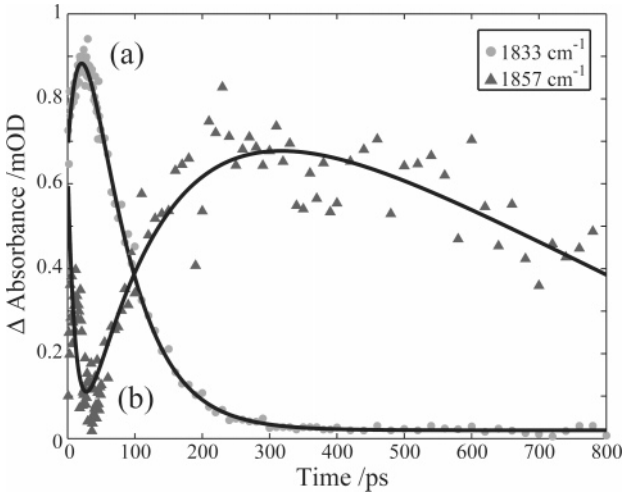

Figure 3. Kinetics of $Ru_3(CO)_{12}$ in cyclohexane excited with 400 nm light: (a) 1833 cm^{-1} peak area and the biexponential fit; (b) 1857 cm^{-1} peak area and corresponding fit.

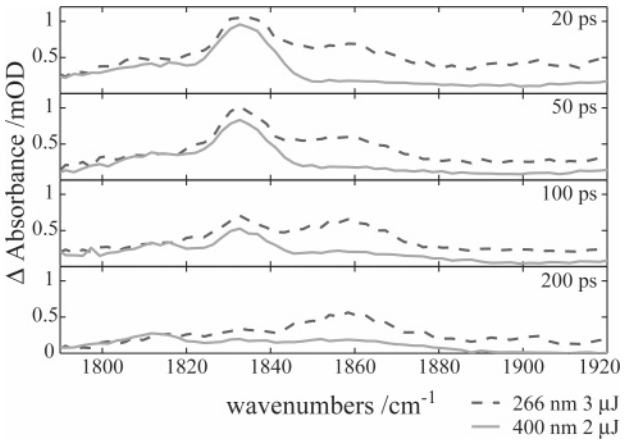

Figure 4. Comparison of spectra when $Ru_3(CO)_{12}$ is excited with 266 nm (dashed line) and 400 nm light (solid line) in cyclohexane. The 400 nm spectra were normalized to the relative intensity of the 266 nm spectra on the basis of a comparison of the 2060 cm^{-1} bleach for both excitation wavelengths.

IR difference spectra for $Ru_3(CO)_{12}$ in cyclohexane excited with 266 nm light are similar to the 400 nm spectra (see the Supporting Information, Figure S1). Kinetics of the transient species (Supporting Information, Figure S2) are reported in Table 1 and are similar to those measured for the photoproducts of 400 nm excitation. In Figure 4 spectra after 266 and 400 nm excitations have been superimposed in order to illustrate their differences. The 400 nm excitation spectra in Figure 4 have been normalized according to the difference in size between the 266 and 400 nm bleach intensity. Bleach intensities can only provide an estimate of the relative quantum yield for reactant depletion at each excitation wavelength, as product peaks overlap with the bleach, but comparing spectra using the bleach intensities appears to be sufficient for a qualitative interpretation of the data. It is apparent from the figure that the peak at 1857 cm^{-1} is larger when 266 nm light was used to excite the cluster. In fact the 1857 cm^{-1} peak was ca. 70% larger when 266 nm light was used rather than 400 nm light, whereas the 1833 cm^{-1} peak was only ca. 18% larger when photoexcited with 266 nm light, relative to 400 nm excitation. As will be discussed later, the peak at 1833 cm^{-1} is assigned to the transient formed as a result of metal−metal bond cleavage and the peak at 1857 cm^{-1} to the transient formed upon CO dissociation.

(b) THF Results. IR difference spectra for $Ru_3(CO)_{12}$ in THF photoexcited with 400 nm light are presented in Figure 5. The large peaks between 1930 and 2100 cm^{-1} represent the IR absorptions of the terminal carbonyls; their recovery times were measured using the trace-fitting method and are reported in Table 2. Unlike the spectra collected in cyclohexane (Figure 2 inset), in THF there appears to be only one small peak at 1833 cm^{-1} (Figure 5 inset) that is assigned to a bridging carbonyl. This peak has a rise time of 8 ± 2 ps and a decay of 53 ± 9 ps and appears to shift to higher energy (i.e. blue shift) with a time constant of 124 ± 12 ps (Figure 6). The shift in center frequency could be attributed to the process of vibrational cooling or might be indicative of growth of a second peak on the higher energy side of the peak at 1833 cm^{-1}. Data collected using 266 nm excitation (see the Supporting Information, Figure S3) have a behavior similar to that observed after 400 nm excitation; however, the dynamics were more difficult to capture, as the peak amplitude was considerably smaller as a result of lower pump power.

B. DFT Results. Geometry optimizations and frequency calculations were performed for the starting material $Ru_3(CO)_{12}$

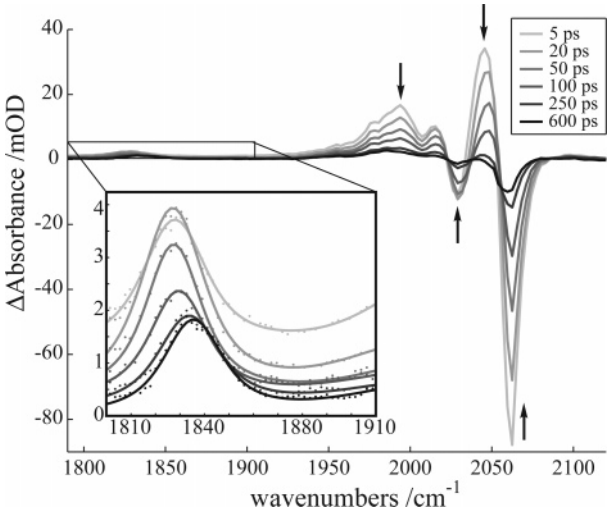

Figure 5. Difference spectra of $Ru_3(CO)_{12}$ excited with 400 nm (0.75 μJ) in a neat solution of THF. Spectra in the inset are fits overlaid on the raw data. Arrows indicate changes with increasing delay time.

Table 2. Kinetics of Product and Bleach Recovery Peaks from $Ru_3(CO)_{12}$ in THF Excited with 266 or 400 nm Light

peak/cm^{-1}	$\tau_{400\ nm}$/ps		$\tau_{266\ nm}$/ps[a]	
	Product Peaks in THF			
1833	8 ± 2	rise		
	53 ± 9	decay		
1890	9 ± 2	decay		
	155 ± 29	decay		
1984	15 ± 2	decay	42 ± 9	decay
	98 ± 6	decay		
1991	17 ± 2	decay	8 ± 5	decay
	98 ± 5	decay	76 ± 15	decay
2016	93 ± 4	decay	110 ± 9	decay
2048	71 ± 1	decay	8 ± 1	decay
			104 ± 5	decay
	Bleach Peaks in THF			
2031	9 ± 1	decay	6 ± 2	decay
	101 ± 1	rise	82 ± 5	rise
2063	25 ± 1	rise	87 ± 3	rise
	101 ± 3	rise		

[a] The signal-to-noise ratio was not sufficient to resolve kinetics for the bridging carbonyl peak at 1833 cm^{-1} or the terminal carbonyl at 1890 cm^{-1} after 266 nm excitation.

and transient species. Figure 7a illustrates the optimized geometry for $Ru_3(CO)_{12}$. Unlike the published crystal structure,[5] these results show a low-symmetry complex in which each metal and its four accompanying carbonyls are tilted by approximately 12−15° off of the plane defined by the three metal atoms. It is likely that in order to increase the packing efficiency the cluster prefers a more symmetric geometry in the crystal, whereas it may tilt in the gas phase to minimize steric interactions. Generally the bond lengths and angles of the calculated gas-phase cluster are quite similar to those of the experimentally measured crystal structure (see Table S1 in the Supporting Information). Calculated frequencies and relative intensities for $Ru_3(CO)_{12}$ (see Table S2 in the Supporting Information) agree well with experimental results reported in this and in previous papers.[3]

The structures for the transient complexes discussed in our experimental work were calculated using DFT and provide the first calculated structures ever reported for these complexes. Solvated and unsolvated forms of the bridging carbonyl complexes are shown in Figures 7 and 8. The bridging carbonyl vibrational frequencies and corresponding amplitudes are listed

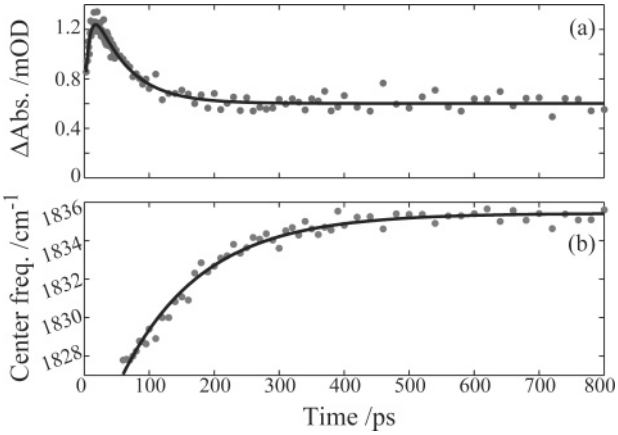

Figure 6. (a) Kinetics of the bridging carbonyl complex of $Ru_3(CO)_{12}$ excited with 400 nm light in THF. Data points correspond to the peak area at each time. (b) Center frequency of the same peak and corresponding monoexponential fit.[33]

in Table 3, and selected structural parameters are listed in Table 4. A complete list of the calculated vibrational frequencies can be found in Tables S2 and S3 in the Supporting Information. Calculated thermodynamic stabilities of the complexes relative to that of the parent complex, $Ru_3(CO)_{12}$, are listed in Table 5. Unsolvated forms of the transients were calculated using both basis sets A and B, and it was found that the structures were similar at both levels of theory; therefore, only basis set A was used for the solvated complexes.

The structure for the metal−metal-cleaved complex (**I**) is shown in Figure 7b. This structure was found by stepwise increases in the length of one Ru−Ru bond followed by geometry optimization at each step to locate the energetic minimum. The optimized structure has a bridging CO spanning two metals that are still bonded (labeled Ru2 and Ru3 in Figure 7b). In contrast, all previous suggestions for the structure of complex **I** hypothesized that the CO would span the gap between the two metals with the broken bond so that the cluster could maintain an 18-electron count at each metal center.[6−8,10,16] Although the structure for **I** does not maintain an even electron count on every metal, this new structure for **I** will be more susceptible to solvation at Ru1, thereby increasing its stability. The bond between Ru1 and Ru2 in complex **I** is lengthened with respect to the Ru1−Ru2 bond in the parent complex and leads us to believe that if a strong π-acceptor solvent molecule were to bind to Ru1, the cluster could easily fragment into a solvated monomer and bridged CO dimer, as was previously observed.[10]

Propane- and THF-solvated forms of **I** were calculated and are shown in parts c and d of Figure 7, respectively. In all cases, the solvent molecule is coordinated to Ru1, the metal center that is lacking a bridging carbonyl. Attempts to calculate a solvated complex in which the solvent molecule is coordinated to Ru3 have failed, leading us to conclude that the best site for solvation is at the coordinatively unsaturated metal center Ru1. When the metal to bridging CO distances are compared for Ru2 and Ru3 (Ru3−C4 and Ru2−C4), it is evident that the bridging carbonyl is almost equidistant between the two metals with a small tendency toward Ru2 (see Table 4). It appears that the type of solvent has only a small effect on the local structure of the bridging carbonyl and the vibrational frequency (Table 3), probably because the site for solvation is two metals away from the bridging carbonyl. The calculated stabilities of the solvated complexes indicate that the THF-solvated complex is more stable than the propane-solvated form (Table 5). Correspond-

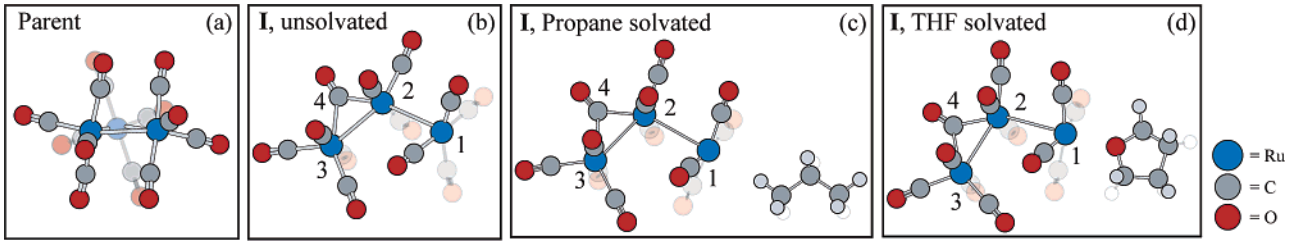

Figure 7. DFT-optimized structures using basis set A (lighter colored atoms are meant to provide a sense of depth and are behind the darker colored atoms): (a) $Ru_3(CO)_{12}$ prior to excitation; (b) $Ru_3(CO)_{12}$ with one metal−metal bond cleaved (**I**); (c) complex **I** solvated with propane; (d) complex **I** solvated with THF.

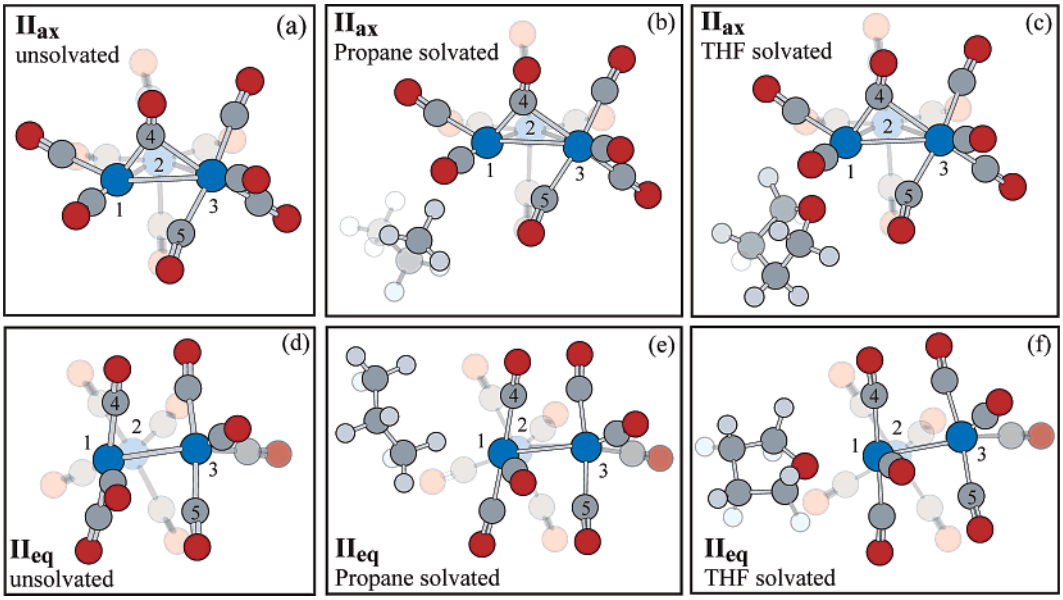

Figure 8. DFT-optimized structures for the CO loss complex: (a) unsolvated complex $\mathbf{II_{ax}}$; (b) $Ru_3(CO)_{10}(\mu\text{-CO})$ formed from axial CO dissociation and solvated with propane; (c) as in (b), except solvated with THF; (d) unsolvated complex $\mathbf{II_{eq}}$; (e) $Ru_3(CO)_{11}$ formed from equatorial CO loss and forms of $\mathbf{II_{eq}}$ solvated with propane; (f) as in (e), except solvated with THF.

Table 3. Vibrational Frequencies (cm^{-1}) and Relative Amplitudes for the Bridging Carbonyl Group in the Unsolvated and Solvated Forms of Complexes I and II_ax

	I	**II_{ax}**[a]
unsolvated, basis set B	1840 (0.39)	1862 (0.18)
unsolvated[b]	1859 (0.34)	1884 (0.18)
propane solvated	1847 (0.27)	1879 (0.21)
THF solvated[c]	1838 (0.19)	1886 (0.16)

[a] Complex $\mathbf{II_{eq}}$ was found to have no bridging carbonyls. [b] Unless otherwise specified, basis set A was used for all calculations. [c] THF-solvated complexes are solvated by the oxygen atom of the THF molecule.

ingly the metal−solvent distance decreases from propane to THF, indicative of a stronger interaction with THF.

DFT calculations have been done for the two possible geometries for the CO loss transients, an axial CO loss and an equatorial CO loss species (Figure 8). When an axial carbonyl was removed from the starting complex, $Ru_3(CO)_{12}$, the bridging carbonyl complex, shown in Figure 8a, complex $\mathbf{II_{ax}}$, was found to be the lowest energy structure. From the vibrational frequencies and the structure, it is clear that there is at least one bridging carbonyl spanning metals 1 and 3 (Table 4), labeled C4. Inspection of the distances between Ru1−C4 and Ru3−C4 indicate that the bridge is asymmetric with bond lengths of 1.915 and 2.415 Å, respectively. The bridging carbonyl vibrational frequency at 1884 cm^{-1} (1862 cm^{-1} with basis set B) corresponds to the stretch of only this carbonyl group. In addition, there is a terminal carbonyl with partial bridging character, labeled C5 in Figure 8a. The bridging for C5 is quite asymmetric, with the stronger, shorter bond being between C5 and Ru3. The vibrational frequency for this carbonyl group is 1954 cm^{-1}, which is higher than most bridging carbonyl frequencies. However, the carbonyl group labeled C5 is closer to the Ru1 metal center in complex $\mathbf{II_{ax}}$ as compared to the case for the parent complex, and the metal carbonyl angle for Ru3−C5−O5 of 168.4° is more bent than is observed in the parent complex. In summary, there appears to be some interaction between this carbonyl (C5) and the metal center Ru1, although it is difficult to say if it could be considered a fully bridging carbonyl.

It is surprising that the coordinatively unsaturated metal center, Ru1, is donating one of its carbonyls (C4) to form the more significant bridge, because this metal center is the coordinatively unsaturated metal. Inspection of the charge distribution among the three metal centers shows that Ru1 is considerably more positive than Ru2 and Ru3, and therefore, the remaining metals do little to stabilize the coordinatively unsaturated metal center. Despite our efforts to locate another structure with a better distribution of charge among the three metal centers, complex $\mathbf{II_{ax}}$ is consistently the most stable carbonyl loss complex, indicating that stabilization must come from the bridging carbonyls. As noted earlier, the major bridging carbonyl, labeled C4, is asymmetrically bridged (with the Ru1−C4 bond being shorter), allowing some stabilization of the coordinatively unsaturated metal center Ru1. In addition, it is likely that the second weakly bridging carbonyl (C5) provides some added stability to Ru1.

Table 4. Calculated Structural Parameters of the Parent Molecule, $Ru_3(CO)_{12}$, as Well as Solvated and Unsolvated Forms of the Transient Complexes I, II_ax, and II_eq

	distance (Å)								angle (deg)			
complex[a] (solvent)	Ru1−C4	Ru3−C4	Ru1−C5	Ru3−C5	Ru1−Ru3	Ru1−Ru2	Ru2−Ru3	Ru1−solv[b]	Ru1−C4−Ru3	Ru1−C5−Ru3	Ru1−C4−O4	Ru3−C5−O5
parent	1.969	3.199	3.203	1.970	2.925	2.925	2.923	NA	63.8	63.7	173.1	173.0
II_{ax}	1.915	2.415	2.489	1.984	2.854	2.822	2.946	NA	81.6	78.4	150.3	168.4
II_{ax} (propane)	1.918	2.397	2.528	1.984	2.866	2.820	2.948	2.938	82.4	77.8	150.0	168.3
II_{ax} (THF)	1.910	2.488	2.527	1.980	2.914	2.879	2.922	2.468	81.9	79.5	154.5	161.9
II_{eq}	1.945	3.230	3.160	1.976	2.843	2.938	2.897	NA	60.8	62.3	174.8	175.1
II_{eq} (propane)	1.949	3.255	3.190	1.974	2.845	2.940	2.915	2.216	60.2	61.6	174.5	174.3
II_{eq} (THF)	1.953	3.307	3.226	1.971	2.855	2.950	2.928	2.350	59.3	61.1	174.2	174.1
I	2.205[c]	2.054			4.980	3.190	2.918	NA	86.4[d]			
I (propane)	2.212[c]	2.043			4.960	3.232	2.946	2.691	87.5[d]			
I (THF)	2.219*c*	2.042			4.981	3.226	2.979	2.431	88.6[d]			

[a] Atom numbers correspond to labels in Figures 7 and 8. [b] In the case of propane, the Ru1-solvent distances are measured from the metal to the hydrogen. For THF, the Ru1−solvent distance is measured from the oxygen. [c] Ru3−C4. [d] Ru3−C4−Ru2.

Table 5. Stability of Calculated Complexes Relative to the Parent Structure, $Ru_3(CO)_{12}$

	$\Delta H°$	
complex (solvent)	basis set A[b]	basis set B[c]
I	23.8	23.9
I (propane)	24.2	24.9
I (THF)	19.5	19.2
II_{ax}	26.5	23.8
II_{ax} (propane)	26.3	
II_{ax} (THF)	19.7	
II_{eq}	33.9	31.2
II_{eq} (propane)	31.2	
II_{eq} (THF)	22.5	

[a] Smaller values indicate a more stable complex. [b] All enthalpies are reported in kcal mol^{-1} and calculated at 298 K. [c] Standard enthalpies calculated from basis sets A and B are similar, and only a few calculations at the higher basis set were performed to illustrate this point.

In the case of the CO loss complex, it is first necessary to determine whether an axial or equatorial CO is dissociated. It was suggested by Bentsen et al. that an equatorial CO is initially photodissociated and that the complex rapidly isomerizes to an axially vacant structure at 110 K.[3] We performed DFT calculations on an equatorially vacant cluster and found that the resulting structure lacks bridging carbonyls (Figure 8d, structure **II_{eq}**). The Ru3−C4 and Ru1−C5 distances for **II_{eq}** are substantially longer than those observed for **II_{ax}**. The Ru−C−O bond angles for **II_{eq}** are quite similar to those observed for the parent molecule. Finally, the lowest carbonyl vibrational frequency at 1963 cm^{-1} consists of antisymmetric vibrations from the four axial carbonyls on Ru1 and Ru2, rather than a single carbonyl stretch as was observed for the major bridging carbonyl in **II_{ax}**. This is consistent with Bentsen et al.'s observation that the **II_{eq}** lacks bridging carbonyls.[3]

The axial vacant complex, **II_{ax}**, is more stable than the equatorially vacant complex, **II_{eq}**, by 7.4 kcal mol^{-1} (Table 5); therefore, isomerization of the complex to an axially vacant structure is thermodynamically favorable. The roles of each of these complexes in the context of the experimental results are discussed further in section IV.

The solvated structures of complexes **II_{ax}** and **II_{eq}** were optimized with propane and THF using basis set A, and results are presented in Figure 8 and Tables 4 and 5. In the case of complex **II_{ax}**, the input structure for the geometry optimization was the parent complex, $Ru_3(CO)_{12}$, with a solvent molecule in place of one of the axial carbonyls. As can be seen in parts b and c of Figure 8, both the propane- and THF-solvated complexes converged to structures containing a bridging carbonyl. Solvated forms of complex **II_{eq}** are shown in Figure 8 parts e and f and, as with the unsolvated form, the solvated **II_{eq}** complexes contain no bridging carbonyls.

IV. Discussion

A. Photochemistry of $Ru_3(CO)_{12}$ in Noncoordinating Solvents. In these experiments, the spectra measured for the bridging carbonyl region show unique features that have not been observed in any spectra reported previously.[3,10,13] A detailed characterization of the photoproducts of $Ru_3(CO)_{12}$ in cyclohexane is based on the kinetics of the bridging carbonyl peaks and a comparison of the intensities at each pump wavelength. On the basis of their kinetics, one can see that the 1833 cm^{-1} peak and the 1857 cm^{-1} peak are uncorrelated and, hence, result from independent species.

The peak at 1857 cm^{-1} is assigned to the carbonyl loss species, **II_{ax}**. Figure 4 shows that this peak is more prominent when 266 nm light is used as the excitation wavelength. This assignment is based on the fact that, in general, UV absorptions of metal carbonyls lead to CO dissociation[3,10] and electronic absorption studies of $Ru_3(CO)_{12}$ have assigned the UV band to a MLCT state that leads to CO dissociation.[14] In addition, the quantum yields for photosubstitution products, which are generally believed to result from CO loss, were shown previously to increase significantly as the excitation wavelength was shortened, which is consistent with our observations.[7,8]

The dynamics of the 1857 cm^{-1} peak also support its assignment to complex **II_{ax}**. At both excitation wavelengths, 266 and 400 nm, this peak was observed to grow in with a time constant of 134−158 ps and remain constant out to 800 ps. It is expected that the bridging carbonyl complex will survive until it recombines with the dissociated CO (in noncoordinating solvents). The rate for CO/cluster recombination is limited by the rate of diffusion and the weak binding strength of the alkane and will occur in the time frame of microseconds.[8]

The peak at 1833 cm^{-1} is assigned to the metal−metal bond cleavage complex **I**. The wavelength comparison study presented in Figure 4 shows that the intensities of the 1833 cm^{-1} peak are similar for both pump wavelengths. This is in agreement with previous studies in which the photofragmentation quantum yields (in coordinating solvents) were found to be wavelength independent.[7,8,10] The dynamics of this peak are consistent with our assignment. The complex was observed to form quickly (15−23 ps) and decay quickly (60−63 ps). It is expected that the product of metal−metal cleavage is short-lived, because the two metals are hinged together by the third and cannot diffuse away, resulting in fast recombination.

The small peak at 1815 cm^{-1} cannot be definitively assigned because of the low signal-to-noise ratio. One can see from inspection of the spectra in Figure 2 that the small peak at 1815 cm^{-1} is long-lived, like its neighbor at 1857 cm^{-1}. This similarity in behavior leads us to believe that the 1815 cm^{-1} peak may be attributed to a CO loss complex. In this case, there may be another configuration for complex **II** that we are unable to locate using DFT.

The simultaneous observation of both **I** and $\mathbf{II_{ax}}$ was overlooked in previous studies, due to limitations in time resolution or detection sensitivity. In the matrix studies by Bentsen et al. it was observed that photofragmentation was blocked by the matrix.[3] If complex **I** was formed in the matrix studies, it may have re-formed the starting material before IR spectra could be collected.[3] In the solution-phase flash photolysis study by Grevels et al. the instrument response time was 80 ns, exceeding the lifetime of complex **I** by 3 orders of magnitude.[10] In the ultrafast vis-pump IR-probe study by Vergeer et al. only complex **I** was observed to form.[13] It is likely that complex $\mathbf{II_{ax}}$ was not observed in this study because the excitation intensity or the detection sensitivity was not sufficient; as can be seen in Figure 4, the peak at 1857 cm^{-1} is barely discernible when a low pump power is used.[26] In Vergeer's study, the 1833 cm^{-1} peak assigned to complex **I** was reported to have a rise time of 3.9 ± 0.9 ps in *n*-heptane solvents;[13] this is faster than the rise times measured in our experiments. This disparity may be attributed to different methods for kinetic fitting, as it is difficult to distinguish peaks at early times after photoexcitation because the broad and intense terminal carbonyl peaks are overlapping the bridging carbonyl absorption(s). The decay time we measured for the 1833 cm^{-1} absorption (60−63 ps) is consistent with the decay time measured by Vergeer et al. (56.6 $\pm$ 6 ps), and this lends support to both of our assignments.

DFT calculations of **I** predict a bridging CO vibrational frequency of 1840 cm^{-1}, whereas $\mathbf{II_{ax}}$ has a calculated vibrational frequency of 1862 cm^{-1} (basis set B, Table 3). This is consistent with the relative positions of **I** and $\mathbf{II_{ax}}$ observed experimentally. In addition, DFT predicts that **I** exhibits a relative peak amplitude that is 2.1 times larger than that of $\mathbf{II_{ax}}$.[27] It is difficult to draw direct comparisons of relative peak amplitudes from the experimental data, since it is not known whether the quantum yields for **I** and $\mathbf{II_{ax}}$ are identical; however, in all experiments (at either 266 or 400 nm pump and at a variety of pump powers) the peak for **I** is considerably larger than that for $\mathbf{II_{ax}}$.

Our DFT studies are also consistent with Bentsen and Wrighton's work, in which they demonstrated that a transient is formed from the photodissociation of an equatorial CO. They were only able to trap the equatorially vacant complex in a matrix of 2-MeTHF at 90 K, and the complex did not contain bridging carbonyls.[3] Similarly, the calculated structure for $\mathbf{II_{eq}}$ lacks bridging carbonyls. Bentsen and Wrighton identified $\mathbf{II_{eq}}$ at 90 K and observed that it rearranges to $\mathbf{II_{ax}}$ upon warming the matrix to 110 K.[3] Our calculations indicate that $\mathbf{II_{ax}}$ is considerably more stable than $\mathbf{II_{eq}}$, thus providing a thermodynamic driving force for this isomerization. It is likely that $\mathbf{II_{eq}}$ is formed prior to $\mathbf{II_{ax}}$ in our experiments, which explains why it takes an average of 139 ± 19 ps to form $\mathbf{II_{ax}}$; however, no feature in our spectra can be positively attributed to $\mathbf{II_{eq}}$, as it contains no bridging carbonyls, and the terminal carbonyl bands will overlap with those of the parent, complex **I**, and complex $\mathbf{II_{ax}}$.

There are a variety of theories that can be applied to this system in order to explain why both **I** and $\mathbf{II_{ax}}$ form simultaneously at a single excitation wavelength. The first theory is that excitation of $Ru_3(CO)_{12}$ populates both MLCT and $\sigma^* \leftarrow \sigma$ states directly. The MLCT (UV) band for $Ru_3(CO)_{12}$ is considerably larger than the $\sigma^* \leftarrow \sigma$ (vis) band; therefore, excitation of the cluster at 400 nm may directly populate the MLCT due to the overlap of the two bands. However, at 266 nm the tail of the absorption band for the $\sigma^* \leftarrow \sigma$ transition is expected to be extremely small and it is not likely that the wavelength-independent quantum yield for the metal−metal bond cleavage channel results from overlapping UV and visible absorption bands. A second possibility, suggested by Desrosiers et al., is that after excitation with UV light the MLCT state associated with the CO loss channel is initially populated and the lower energy σ^* state associated with the metal−metal cleavage channel is subsequently populated via internal conversion.[8] The process of internal conversion can be as fast as a few hundred femtoseconds,[28] and this seems to be a reasonable explanation for the observation of two channels at short wavelengths. A third explanation is that excitation into the σ^* state and subsequent rearrangement of the molecular geometry results in an energetic lowering of the electronic states associated with the CO loss channel, as was observed for $Mn_2(CO)_{10}$.[29] Finally, the dipole-forbidden transition predicted by Delley and co-workers to be energetically equal to the $\sigma^* \leftarrow \sigma$ transition may result in weakening of the metal carbonyl bond.[15]

B. Photochemistry of $Ru_3(CO)_{12}$ in THF. The bridging carbonyl complex(es) observed in THF are the first ever reported under ambient conditions. Previous studies of the photoinduced dynamics of $Ru_3(CO)_{12}$ in THF have shown that a THF molecule solvates and stabilizes the photoproducts, but no study has conclusively demonstrated whether these complexes contain bridging carbonyls.[3,8,9] This is important, because understanding the nature of the photoproducts improves our understanding of the subsequent chemistry of these complexes.

In the spectra collected for $Ru_3(CO)_{12}$ in THF it is not obvious whether there is one peak that shifts its position or two peaks with different dynamics. If the feature at 1820−1850 cm^{-1} is attributed to a single peak, the peak center shift to higher energy is a consequence of vibrational relaxation, as the time scale is consistent with the time scale for vibrational relaxation of metal hexacarbonyl complexes in alkanes.[30] The dynamics of this peak (Table 2) and its position suggest that it results from a solvated form of species **I**. This assignment is consistent with a previous study in which 395 nm irradiation of $Ru_3(CO)_{12}$ in THF produced a transient with a lifetime of 50 ms that was assigned to a THF-stabilized form of **I**.[8] In this scenario, complex $\mathbf{II_{eq}}$ is likely formed and solvated by THF, consequently preventing the formation of the bridging CO complex $\mathbf{II_{ax}}$.[3]

There is one major inconsistency with the assignment of the 1820−1850 cm^{-1} feature as one peak. The dynamics of the feature indicate that it grows in and decays with rates that are similar to those observed for complex **I** in cyclohexane. However, it does not decay back to the baseline; instead, it

(26) A linear dependence on excitation energy at 400 nm in our experiments confirmed that these peaks result from single photon processes (see the Supporting Information, Figure S4).

(27) In determining the relative amplitude of **I** vs $\mathbf{II_{ax}}$, all the vibrational frequencies for each molecule were internally scaled relative to the strongest vibrational mode in each molecule and then the relative amplitudes of the two molecules were compared using these scaled amplitudes. The vibrational frequencies of these two molecules were also compared by scaling both to the largest vibrational mode of the parent molecule, and the relative amplitude of **I** vs $\mathbf{II_{ax}}$ using this method was 2.9:1.

(28) Vlcek, A. J. *Coord. Chem. Rev.* **2000**, *200−202*, 933.
(29) Baerends, E. J.; Rosa, A. *Coord. Chem. Rev.* **1998**, *177*, 97.
(30) Dougherty, T. P.; Heilweil, E. J. *Chem. Phys. Lett.* **1994**, *227*, 19.

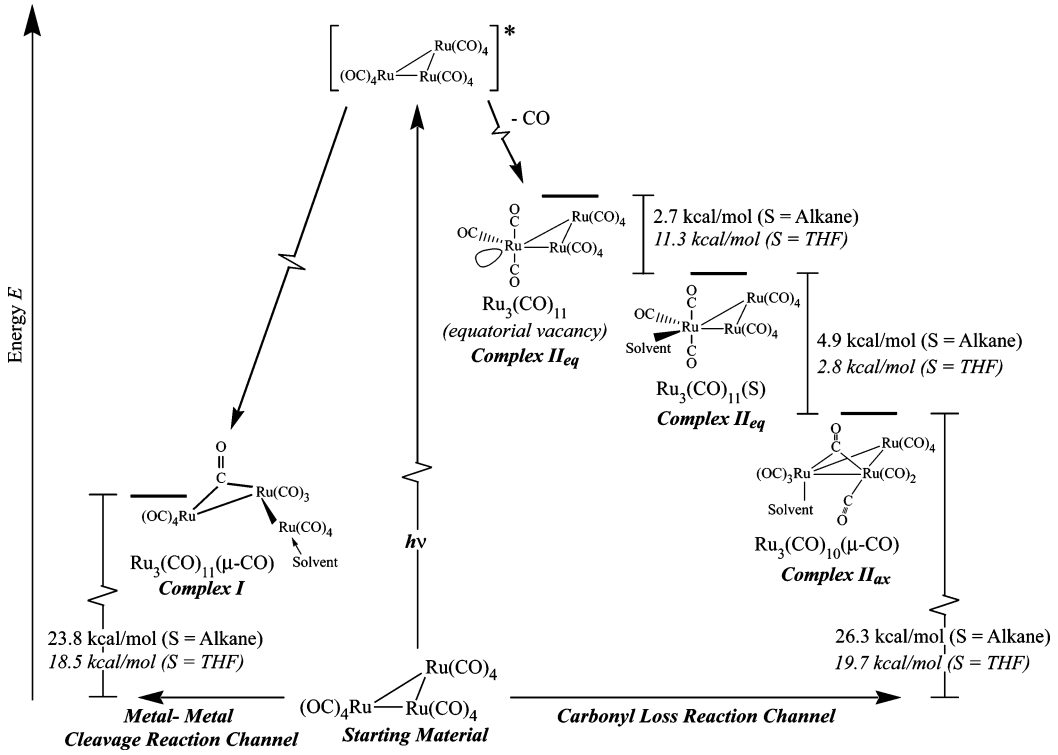

Figure 9. Principal species formed in irradiation of $Ru_3(CO)_{12}$ in cyclohexane and THF. To visualize both reaction channels, the metal−metal cleavage channel is on the left side, whereas the CO loss channel is on the right. The CO loss quantum yield is greater when the cluster is irradiated with 266 nm vs 400 nm, while metal−metal cleavage quantum yields are similar after both 266 and 400 nm irradiation. See the text for details. Energetics of all species were derived from DFT calculations using basis set A.

maintains an amplitude of ca. 0.6 mOD out to 800 ps. There may be two modes of THF solvating the cluster, the first being oxygen solvation that traps complex **I** in its bridged form and the second being alkyl solvation, resulting in some population that is able to recover to the starting material as was observed in cyclohexane. This hypothesis was tested by exploring the photoinduced solvation dynamics of $Cr(CO)_6$ in THF.[31] It was clear from these experiments that, upon CO dissociation, the $Cr(CO)_5$ fragment is solvated by the oxygen group on THF within the time scale of vibrational relaxation and no alkyl-solvated form of $Cr(CO)_5$ was detected. This result is not surprising, since the distance from oxygen to the β-carbons is the same as the distance between the β-carbon and the oxygen in ethanol, a solvent which shows solvation at the hydroxyl group rather than the alkyl chain.[32]

If the feature at 1820−1850 cm^{-1} is actually attributed to two peaks, then the absence of an isosbestic point suggests that the peaks result from unrelated species. On the basis of our DFT results and the dynamics of the feature, the large peak at 1833 cm^{-1} is attributed to complex **I** and the peak at ca. 1840 cm^{-1} is assigned to a THF-solvated form of $\mathbf{II_{ax}}$. The early-time peak position and dynamics for the feature (8 ± 2 ps rise and 53 ± 9 ps decay) are extremely close to the average dynamics observed for **I** in cyclohexane (17 ± 2 ps rise and 61 ± 4 ps decay). At later times, the relative position and long-lived nature of the peak in THF are consistent with the position and dynamics of $\mathbf{II_{ax}}$ in cyclohexane. In this scenario, the center frequency shift (i.e. blue shift) of the feature of $\tau = 124$ ps is attributed to the formation time of the THF-solvated $\mathbf{II_{ax}}$ and is within error of the average formation time of $\mathbf{II_{ax}}$ in cyclohexane (139 ± 19 ps). It seems possible that THF may be able to stabilize $\mathbf{II_{ax}}$ in a nonbridged form, but DFT results clearly indicate that the THF-solvated structure contains bridging carbonyls. It is important to note that the DFT-generated structure for THF-solvated $\mathbf{II_{ax}}$ was found by starting the optimization from the parent complex with one of the axial CO's replaced with THF.

The two peak hypotheses and assignments are further supported by previous work. Matrix studies by Bentsen et al. indicate that a bridging carbonyl complex resulting from CO dissociation forms in a 2-MeTHF matrix; however, they were unable to say whether this complex was solvated by 2-MeTHF.[3] While it has been suggested by Bentsen et al. that the bridging carbonyl complex they observed might be an unsolvated form of $\mathbf{II_{ax}}$,[3] our DFT results clearly indicate that a THF-solvated form of the complex is thermodynamically more favorable (see Table 5). In conclusion, if the feature between 1820 and 1850 cm^{-1} results from two peaks, the peaks at 1833 and 1840 cm^{-1} can be assigned to the THF-solvated forms of **I** and $\mathbf{II_{ax}}$, respectively, on the basis of our cyclohexane and DFT results and previous work. However, an irrefutable assignment of this feature requires better wavenumber resolution in order to determine whether it results from one or two peaks.

V. Conclusions

The dynamics of $Ru_3(CO)_{12}$ after photoexcitation was followed by monitoring the small but distinct infrared absorptions of the bridging carbonyls. The results of these studies are summarized in Figure 9. In both cyclohexane and THF, excitation of $Ru_3(CO)_{12}$ with either 266 or 400 nm light results

(31) Unpublished data.

(32) (a) Kling, M. F.; Glascoe, E. A.; Shanoski, J. E.; Payne, C. K.; Mork, B. V.; Tilley, T. D.; Harris, C. B. To be submitted for publication in *Organometallics*. (b) Shanoski, J.; Glascoe, E.; Harris, C. B. *J. Phys. Chem. B*, in press.

(33) The first 50 ps was removed because an early time low-energy shift of the peak made the longer time high-energy shift difficult to determine. The low-energy shift may result from difficulty in fitting the peak at early times because it is vibrationally excited, very broad, and rather weak in amplitude.

in formation of two photoproducts: the first is a metal−metal cleavage complex (**I**, left side of Figure 9), and the second is a carbonyl loss product (**II**, right side of Figure 9). Complex **I** showed an average formation time of 17 ± 1 ps and an average lifetime of 61 ± 4 ps in cyclohexane. The formation rate for **I** may be correlated with the rate for fast vibrational cooling observed in the terminal carbonyl bands (10−30 ps).

On the basis of our DFT and experimental results as well as previously published results,[3] it is likely that an equatorial CO is dissociated, resulting in formation of $\mathbf{II_{eq}}$ that isomerizes to $\mathbf{II_{ax}}$. The DFT studies have demonstrated that the equatorially vacant cluster ($\mathbf{II_{eq}}$) is unstable relative to its axially vacant isomer ($\mathbf{II_{ax}}$) and contains no bridging carbonyls. Therefore, the bridging carbonyl observed in the experiments can only result from an axially vacant complex. The average formation time for $\mathbf{II_{ax}}$ of 139 ± 19 ps in noncoordinating solvents is likely to involve isomerization from an equatorially vacant to an axially vacant species and subsequent or concomitant bridging of a CO. The lifetime of $\mathbf{II_{ax}}$ is greater than the time scale of our experiment and has been demonstrated by others to depend on the concentration of CO with a rate of decay that is diffusion limited.[9]

In THF, it is impossible to definitively state whether there is one or two bridging carbonyl absorptions; however, because the feature at 1830−1850 cm^{-1} exhibits early time dynamics but does not decay to the baseline, it seems more likely that there are two peaks. In this case, the peaks are likely to result from THF-solvated forms of **I** and $\mathbf{II_{ax}}$. This assignment is supported by our cyclohexane spectra, DFT studies, and previous work.[3,8] It is interesting that, in THF, $\mathbf{II_{ax}}$ forms with a rate that is similar to the formation rate in cyclohexane; if $\mathbf{II_{eq}}$ is solvated and stabilized by THF, one might expect it to be longer lived and slow the formation of $\mathbf{II_{ax}}$. Therefore, it is likely that $\mathbf{II_{ax}}$ formation is also correlated with vibrational cooling, as a vibrationally hot form of $\mathbf{II_{eq}}$ will have sufficient thermal energy to dissociate the solvated THF molecule.

One of the main objectives in our studies was to find out how many bridging carbonyl complexes are formed after UV or visible light excitation of $Ru_3(CO)_{12}$. Prior to the results presented in this paper no study had ever characterized more than one bridging carbonyl complex,[3,10,13] despite the indirect evidence that there must be two forming simultaneously (on the basis of the simultaneous formation of both photofragmentation and photosubstitution products).[7,8,16] Consequently, Grevels and co-workers[10] suggested that the path to photofragmentation after UV excitation of the cluster involved the formation of only one bridging carbonyl complex, $\mathbf{II_{ax}}$, which subsequently underwent photofragmentation. Our studies have resolved that there are two bridging carbonyl complexes formed after excitation at a single wavelength, and the hypothesis that multiple bond cleavage channels are accessed producing multiple photoproducts[7,8] is supported. Our results indicate that Grevel et al.'s favored mechanism for fragmentation after short wavelength excitation is incorrect.[10]

Another objective of our studies was to determine the role of the bridging carbonyl complexes in coordinating solvents. THF was chosen, because it was shown to block photofragmentation without changing photosubstitution yields.[6−8] On the basis of our results it seems most likely that both bridging carbonyl complexes are formed after 400 nm excitation in THF and generally show behavior similar to that observed in cyclohexane. In our studies, complex **I** was extremely short-lived in both THF and cyclohexane (53−63 ps). In cyclohexane we presume that **I** decays back to the starting complex, because longer time studies were never able to characterize a metal−metal cleavage transient in alkane solvents.[8] However, in THF a second transient must be formed that is stabilized by THF and lacks bridging carbonyls, because flash photolysis studies have located a transient formed from long-wavelength irradiation in THF that is absent in alkane solvents.[8] We are currently investigating the nature of the second THF-stabilized transient as well as the role of the bridging carbonyl complex in π-backbonding solvents.

In summary, our combined experimental and theoretical studies provide additional insights into the photochemistry of $Ru_3(CO)_{12}$ complexes and the nature and role of bridging carbonyl intermediates.

Acknowledgment. We thank the National Science Foundation for funding and the Office of Basic Energy Sciences, Chemical Sciences Division, of the U.S. Department of Energy under Contract No. DE-AC02-05CH11231 for the use of some specialized equipment. M.F.K. acknowledges support by the Alexander von Humboldt foundation through a Feodor-Lynen Fellowship.

Supporting Information Available: Figures displaying spectra and kinetics of $Ru_3(CO)_{12}$ excited with 266 nm light in cyclohexane and THF and a plot of power-dependent peak amplitudes for the bridging carbonyl peaks and tables giving DFT calculated structural parameters of the parent $Ru_3(CO)_{12}$ and all vibrational frequencies for the parent $Ru_3(CO)_{12}$ and complexes **I**, $\mathbf{II_{ax}}$, and $\mathbf{II_{eq}}$. This material is available free of charge via the Internet at http://pubs.acs.org.

OM050795O